The inositol polyphosphate 5-phosphatase Ocrl associates with endosomes that are partially coated with clathrin

Alexander Ungewickell*, Michael E. Ward*, Ernst Ungewickell†, and Philip W. Majerus*‡

*Division of Hematology, Washington University School of Medicine, St. Louis, MO 63110; and †Medizinische Hochschule Hannover, Hannover 30625, Germany

Contributed by Philip W. Majerus, August 4, 2004

The subcellular localization of Ocrl, the inositol polyphosphate 5-phosphatase that is mutated in Lowe syndrome, was investigated by fluorescence microscopy. Ocrl was localized to endosomes and Golgi membranes along with clathrin, giantin, the mannose 6-phosphate receptor, transferrin, and the early endosomal antigen 1 endosomal marker in fixed cells. The endosomal localization of Ocrl was confirmed by live-cell time-lapse microscopy in which we monitored the dynamics of Ocrl on endosomes. GST binding assays show that Ocrl interacts with the clathrin terminal domain and the clathrin adaptor protein AP-2. Our findings suggest a role for Ocrl in endosomal receptor trafficking and sorting.

The cellular function of the inositol polyphosphate 5-phosphatase Ocrl, which is mutated in patients with Lowe syndrome, is poorly understood. The complex phenotype of Lowe syndrome includes renal Fanconi syndrome, growth failure, mental retardation, cataracts, and glaucoma (1, 2).

Ocrl is a member of the type II family of inositol polyphosphate 5-phosphatases that hydrolyze the 5-phosphate of inositol-1,4,5-trisphosphate, inositol-1,3,4,5-tetrakisphosphate, phosphatidylinositol-4,5-bisphosphate (PtdIns-4,5-P_2), and phosphatidylinositol-3,4,5-trisphosphate. Other members of this family include type II 5-phosphatase, synaptojanin-1, and synaptojanin-2 (3). The preferred substrate of Ocrl is phosphatidylinositol-4,5-bisphosphate, and this lipid accumulates in kidney proximal tubule cells from Lowe syndrome patients (4). In addition to the 5-phosphatase domain, Ocrl also contains a RhoGap domain and an N-terminal region of unknown function.

Ocrl has been localized to lysosomes in kidney proximal tubule cells and to the trans-Golgi network (TGN) in fibroblasts (4, 5). This localization is consistent with a role for Ocrl in lysosomal enzyme trafficking from the TGN to lysosomes. The activities of several lysosomal hydrolases are elevated in plasma from Lowe syndrome patients compared with age-matched controls (6). Both the Ocrl substrate, PtdIns-4,5-P_2, and its product, phosphatidylinositol-4-phosphate, have been implicated in the regulation of clathrin-coated vesicle (CCV) formation at the TGN (7–9). Mannose 6-phosphate receptor (M6PR)-bound lysosomal enzymes are recruited by AP-1 and GGA proteins into CCVs that transport them from the TGN to endosomes (10). We therefore decided to study whether Ocrl is involved in intracellular trafficking, focusing particularly on the transport of lysosomal enzymes by the M6PR.

In this paper we show that Ocrl interacts with clathrin and colocalizes with clathrin on endosomal membranes that contain transferrin (Tf) and M6PR. By using time-lapse microscopy, we demonstrate that Ocrl and clathrin are associated with rapidly moving endosomal structures that increase dramatically in number and motility after serum stimulation. We also find partial colocalization of Ocrl with clathrin and the M6PR at the TGN, consistent with previous studies localizing Ocrl to the TGN (11). Our data support a role for Ocrl in M6PR trafficking and endosomal sorting.

Materials and Methods

Reagents and Chemicals. All chemicals were purchased from Sigma unless stated otherwise. IgG and protease-free BSA for immunofluorescence (IF) were obtained from Jackson ImmunoResearch.

Antibodies. Clathrin (X.22) and AP-2 (AP.6) antibodies were a gift from Frances Brodsky (University of California, San Francisco). Affinity-purified anti-cation-independent M6PR (CI-M6PR) polyclonal antibody was kindly provided by Stuart Kornfeld (Washington University Medical School). A rabbit antibody raised against the N-terminal peptide EPPLPVGAQPLATVE(C) was used for Ocrl Western blotting. Monoclonal early endosomal antigen 1 (EEA1), synaptotagmin, and AP-1 γ appendage subunit (AP-1γ) antibodies were purchased from BD Biosciences. Polyclonal giantin antibody and monoclonal GFP antibody were purchased from Covance (Princeton). Monoclonal hepatocyte growth factor-regulated tyrosine kinase substrate antibodies were purchased from Alexis Biochemicals (San Diego). Monoclonal M2 anti-flag antibody was obtained from Sigma. Tf-Alexa 555, Tf-Alexa-568, secondary fluorescent antibodies, and mounting media were purchased from Molecular Probes.

Rat Brain Fractionation. The coated vesicle purification was performed as described in refs. 12 and 13. The fractions were a gift from R. Bauerfeind (Medizinische Hochschule Hannover).

Protein Purification. Recombinant Ocrl and Ocrl AEANF mutant proteins were purified from SF9 cells by using a MonoS ion exchange column (Amersham Pharmacia) as described in ref. 4.

Generation of Ocrl cDNA Constructs. All Ocrl constructs were generated from pVL1393-Ocrl (4). The Ocrl cDNA was subcloned into pcDNA3.1+ (Invitrogen) by using *Bam*HI and *Xba*I. The following Ocrl mutants were created by PCR site-directed mutagenesis (QuikChange, Stratagene): Ocrl AEANF (^{151}F to A and ^{153}D to A), Ocrl LIAAA (^{704}D to A, ^{705}L to A, and ^{706}E to A), and Ocrl D499A (^{499}D to A).

GST-Golgi-localized, γ-ear-containing ARF-binding protein 2 (GGA2) (170–613) and GST-γ appendage constructs were

Abbreviations: AP-2α, AP-2 α appendage subunit; AP-1γ, AP-1 γ appendage subunit; CCV, clathrin-coated vesicle; CD-M6PR, cation-dependent mannose 6-phosphate receptor; CFP, cyan fluorescent protein; CI-M6PR, cation-independent mannose 6-phosphate receptor; DsRed, *Discosoma* sp. red fluorescent protein; EEA1, early endosomal antigen 1; GGA2, Golgi-localized, γ-ear-containing ARF-binding protein 2; IF, immunofluorescence; M6PR, mannose 6-phosphate receptor; PtdIns-4,5-P_2, phosphatidylinositol-4,5-bisphosphate; TD, clathrin terminal domain; Tf, transferrin; TGN, trans-Golgi network.

‡To whom correspondence should be addressed. E-mail: phil@im.wustl.edu.

kindly provided by Stuart Kornfeld. Cyan fluorescent protein (CFP)-cation-dependent-M6PR (CD-M6PR) was a gift from Suzanne Pfeffer (Stanford University, Stanford, CA). Lois Greene (National Institutes of Health, Bethesda) kindly provided the CFP-clathrin light chain construct. GST-clathrin terminal domain (TD) and *Discosoma* sp. red fluorescent protein (DsRed)-Clathrin light chain were kindly provided by Jim Keen (Thomas Jefferson University, Philadelphia).

GST Binding Assays and Western Blotting. GST or GST fusion protein (100 μg) was bound to glutathione beads (Amersham Biosciences) and incubated with ≈500 ng of Ocrl or Ocrl AEANF mutant protein in assay buffer [25 mM Hepes, pH 7.2/125 mM potassium acetate/2.5 mM magnesium acetate/1 mM DTT/0.4% Triton X-100/complete protease inhibitor mix (Roche, Gipf-Oberfrick, Switzerland)] on a rotator at 4°C overnight. Beads were washed four times with assay buffer before 2× sample buffer was added.

GST-TD beads were incubated with lysates of HeLa cells transfected with Flag or GFP-tagged Ocrl in 10-cm plates. Cells were washed with PBS and then lysed on ice for 5 min in 25 mM Hepes (pH 7.2)/100 mM NaCl/1 mM DTT/0.1% Saponin/complete protease inhibitor mix (Roche). Lysates were centrifuged for 15 min at 90,000 × *g* in a TLA 45 rotor in a TL100 benchtop ultracentrifuge (Beckman Coulter). The final volume of lysate was 3 ml per plate. Cytosol (750 μl) was incubated with GST-TD or GST beads. The mixture was incubated on ice for 1 h and stirred manually every 5–10 min. Beads were pelleted and washed once with lysis buffer without Saponin. Beads were spun through a 10% sucrose cushion, washed once with lysis buffer, and resuspended to a final volume of 90 μl. Ninety microliters of beads and 90 μl of unbound fraction (supernatant) were boiled in sample buffer, and 15 μl was loaded onto an SDS/PAGE gel.

For Western blots, all primary antibodies were diluted in PBS with 0.1% Tween 20/5% BSA/0.02% NaN_3. Secondary antibodies (Pierce) were diluted in 5% dry milk/PBS with 0.1% Tween 20.

IF Microscopy. Cells grown on coverslips were fixed for 5 min with IF fixation buffer (10 mM Pipes, pH 6.5/127 mM NaCl/5 mM KCl/1.1 mM NaH_2PO_4/0.4 mM K H_2PO_4/2 mM $MgCl_2$/5.5 mM glucose/1 mM EGTA/4% paraformaldehyde) and then washed with Tris-buffered saline and solubilized with 0.5% Triton X-100 in PBS for 10 min. Primary and secondary antibodies were diluted in PBS/0.1% Triton X-100/5% BSA. Cells were incubated for 1 h with primary antibodies and for 30 min with secondary antibodies at 37°C. Washes after antibody incubations were performed by dipping coverslips into PBS 30 times. Cells were mounted in Prolong mounting media (Molecular Probes).

Transient Transfections. HeLa or Cos7 cells were transfected with Lipofectamine 2000 (Invitrogen) according to the manufacturer's instructions. All experiments were performed 1–3 days after transfection.

Live-Cell Fluorescence Microscopy. Cos7 cells were transfected and cultured in DMEM plus 10% FBS. Eight hours after transfection, cells were trypsinized and plated on 25-mm glass coverslips (assistant grade, Carolina Biological Supply) at 2×10^4 cells per coverslip. Twelve hours after transfection, cells were transferred to DMEM plus 0.1% BSA and serum-starved overnight. Cells were imaged between 24 and 36 h posttransfection. For imaging, coverslips were transferred to a custom-built coverslip holder, overlayed with 500 μl of Leibovitz's L15 medium plus 0.1% BSA, and transferred to the stage of a Nikon Eclipse TE2000-S inverted microscope. The coverslip holder was then covered with a 60-mm Petri-dish lid to prevent evaporation. The microscope was fitted with a custom-built acrylic incubating chamber to maintain a constant 37°C imaging environment. For all experiments, a 60 × 1.4 numerical aperture oil-immersion objective and 37°C immersion oil (Cargille Type 37, SPI Supplies, West Chester, PA) were used. Images were captured by using a Coolsnap-ES camera (Roper Scientific, Tucson, AZ). Exposure of cells to light was minimized by using a computer-controlled mechanical shutter (Lambda 10–2, Sutter Instruments, Novato, CA) placed in the excitation light path. For simultaneous imaging of CFP, GFP, and DsRed/Alexa 568, a single dichroic mirror was used (86006, Chroma Technology, Rockingham, VT), and excitation and emission filter wheels (Lambda 10–2, Sutter Instruments) were used to change excitation and emission filters. METAMORPH software (Universal Imaging, Downingtown, PA) was used to control all imaging components and for postacquisition image analysis. For serum stimulation of cells, 500 μl of 37°C Leibovitz's L15 medium plus 20% FBS was added to the coverslip chamber and mixed with the existing Leibovitz's L15 medium by gently pipetting up and down.

Results

GFP-Ocrl Localizes to Perinuclear Golgi Membranes and Endosomes. When expressed at low to moderate levels in Cos7 cells, the bulk of GFP-Ocrl localizes to perinuclear membranes, consistent with a Golgi localization first described by Olivos-Glander *et al.* (14). Giantin, AP-1, CI-M6PR, and clathrin partially colocalize with GFP-Ocrl (Fig. 1 and data not shown). Interestingly, we also observed peripheral GFP-Ocrl punctae that overlap with EEA1, clathrin, and endocytosed Tf, indicating that Ocrl is located on endosomes (Fig. 1).

At high expression levels, GFP-Ocrl causes a redistribution of AP-1 and the CI-M6PR. Expression of GFP-Ocrl D499A, a mutant with no phosphatase activity (15), has the same effect (Fig. 6, which is published as supporting information on the PNAS web site). High levels of GFP-Ocrl expression can also result in the redistribution of the Golgi stack marker giantin (data not shown), indicating that Ocrl overexpression can even interfere with the structural organization of the Golgi apparatus.

Time-Lapse Microscopy of GFP-Ocrl in Cos7 Cells Reveals Punctae of Vesicular GFP-Ocrl That Increase in Number and Motility upon Serum Stimulation. To characterize the subcellular localization of Ocrl further, we decided to image GFP-Ocrl *in vivo*. Cos7 cells were transiently transfected with GFP-Ocrl and serum-starved overnight in DMEM/0.1% BSA. The cells were imaged the following day (Movies 1 and 2, which are published as supporting information on the PNAS web site). Fig. 2 shows the strong Golgi localization of GFP-Ocrl and relatively few peripheral punctae before serum stimulation. Upon serum stimulation, a large increase in the number of peripheral GFP-Ocrl-positive structures was observed. Interestingly, GFP-Ocrl is only seen on a subset of vesicular structures. Some Ocrl-negative vesicular structures accumulate Ocrl after serum stimulation (Fig. 2 *Inset*). Two types of Ocrl-positive structures are present: individual punctae and larger vesicular structures that contain Ocrl around the rim. Many of the larger Ocrl-containing vesicles also contain one or more punctae of Ocrl accumulation along their membrane (Fig. 2 *Inset*). We sometimes observe fusion events in which the small Ocrl punctae dock to the larger vesicular structure and stay associated with them along the rim for up to 30 s. Small Ocrl punctae can also be seen leaving the larger structures.

Based on IF analysis of fixed cells that showed that GFP-Ocrl colocalizes with EEA1, clathrin, and internalized Tf, those peripheral structures are probably endosomes (Fig. 1). Tf is known to localize to clathrin-coated pits, early endosomes, and recycling endosomes. To determine whether the GFP-Ocrl-positive structures are identical to the highly motile clathrin-

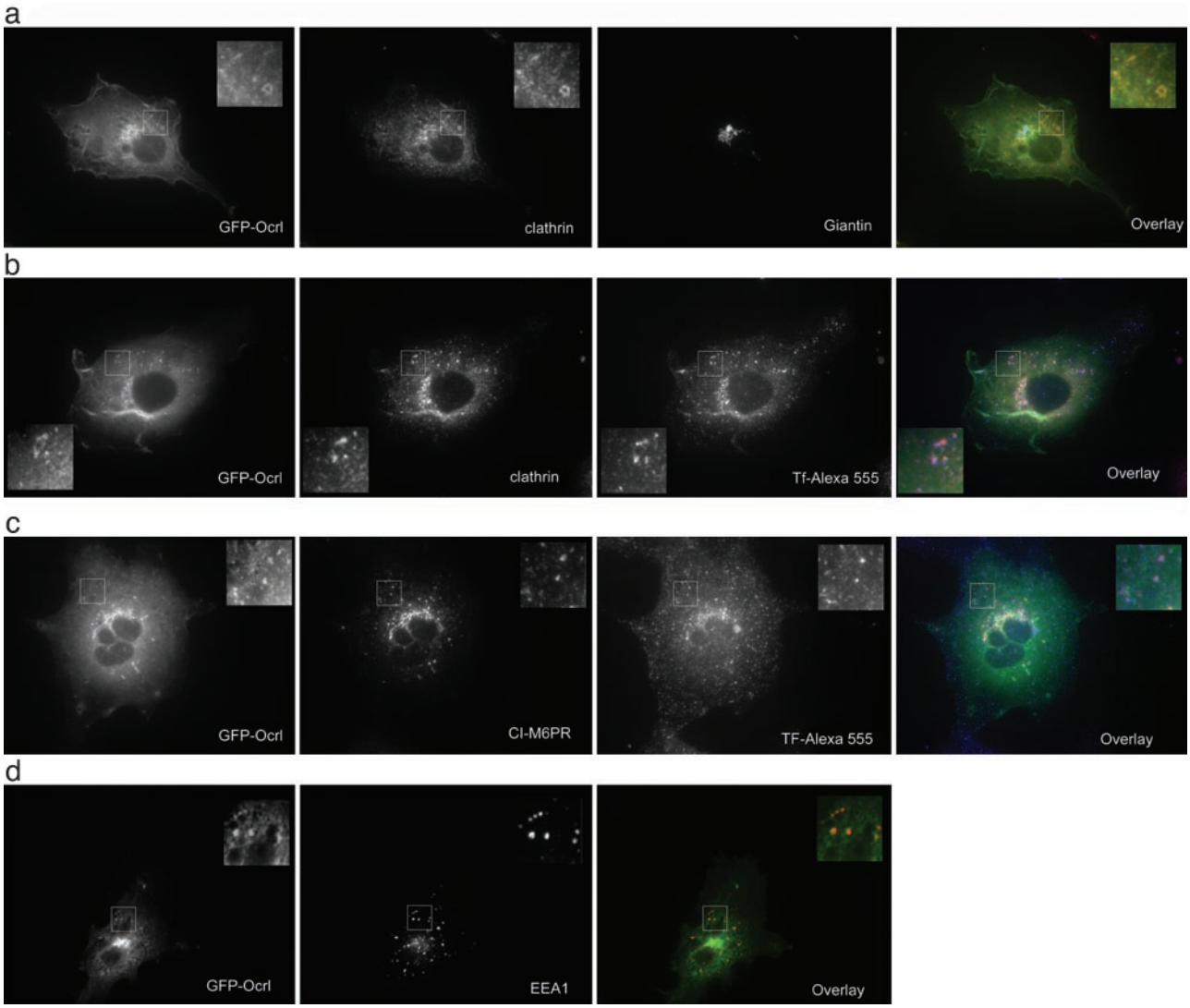

Fig. 1. IF microscopy of Cos7 cells transiently transfected with GFP-Ocrl. Cells in *a–c* were serum-starved overnight in DMEM/0.1% BSA and serum-stimulated for 5 min before fixation. Cells in *b* and *c* were loaded for 30 min with 50 μg/ml Tf-Alexa 555 before serum stimulation. (*a*) GFP-Ocrl with clathrin and giantin stain. Overlay includes GFP-Ocrl (green), clathrin (red), and giantin (blue). (*b*) GFP-Ocrl-expressing cells were loaded with Tf-Alexa 555 and stained for clathrin. Overlay includes GFP-Ocrl (green), clathrin (red), and Tf (blue). (*c*) GFP-Ocrl-expressing cells were loaded with Tf-Alexa 555 and stained for the CI-M6PR. Overlay includes GFP-Ocrl (green), CI-M6PR (red), and Tf (blue). (*d*) GFP-Ocrl-expressing cells were stained for EEA1. Overlay includes GFP-Ocrl (green) and EEA1 (red).

positive endosomal structures that were recently described by total internal reflection microscopy (16), we decided to image Ocrl, clathrin, and Tf in live cells.

Time-Lapse Microscopy Shows Moving Endosomal Structures Containing CFP-Clathrin, GFP-Ocrl, and Tf-Alexa 568. Cos7 cells were cotransfected with CFP-clathrin light chain and GFP-Ocrl and were serum-starved overnight. About 24 h after transfection, cells were incubated in 50 μg/ml Tf-Alexa 568 DMEM/0.1% BSA for 30 min. Sequential images of the three fluorophores were taken before and after serum stimulation. Images in Fig. 3*a* that were taken after serum stimulation show that CFP-clathrin, GFP-Ocrl, and Tf-Alexa 568 are localized on the same structures and move together in the cytoplasm (Movie 3, which is published as supporting information on the PNAS web site). This is the case for both the smaller GFP-Ocrl punctae and the larger vesicular structures. Almost all GFP-Ocrl-positive structures contain Tf, but only a subset of Tf punctae contain GFP-Ocrl. Similar to GFP-Ocrl (Fig. 2), the number of CFP-clathrin punctae also increases upon serum stimulation (data not shown). Furthermore, we observed that Ocrl and clathrin often overlap on the endosomal membranes and that Tf is clearly associated with the same structures. Because the endosomes move rapidly and the different fluorophores were imaged sequentially, Ocrl and clathrin do not always overlap on the merged images even though they are on the same structure (Fig. 3*a* and Movie 3, 19 s CFP-clathrin–GFP-Ocrl merge).

The live imaging thus confirms the colocalization of Ocrl and clathrin on Tf-Alexa-555-positive endosomes in fixed Cos7 cells (Fig. 1*b*). To address our original hypothesis that Ocrl is involved in the trafficking of lysosomal enzymes, we decided to image Ocrl, clathrin, and the M6PR in Cos7 cells upon serum stimulation.

Time-Lapse Microscopy Reveals Colocalization of GFP-Ocrl, CFP-CD-M6PR, and dsRed-Clathrin on Endosomes. GFP-Ocrl, CFP-CD-M6PR, and dsRed-clathrin were transfected into Cos7 cells and analyzed 24 h after transfection upon serum stimulation by time-lapse microscopy. GFP-Ocrl, CFP-CD-M6PR, and dsRed-clathrin generally colocalize in the Golgi region. Because of the

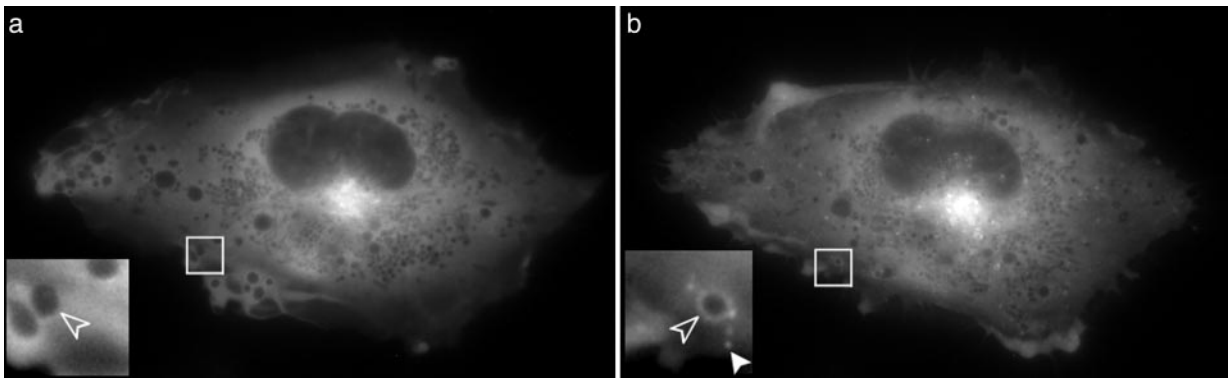

Fig. 2. GFP-Ocrl before (*a*) and 23 min after (*b*) serum stimulation. A large increase in the number of peripheral GFP-Ocrl punctae (solid arrowhead) and rings (open arrowhead) was observed after serum stimulation. Not all vesicular structures contain Ocrl, and some acquire Ocrl upon serum stimulation (open arrowheads) (see Movie 1).

thickness of the cells in the perinuclear regions, we were unable to see vesicular structures leaving the TGN. We did observe that CFP-CD-M6PR was present in GFP-Ocrl- and dsRed-clathrin-positive endosomal structures. As shown in Fig. 3*b*, all three proteins move together on these endosomes (Movie 4, which is published as supporting information on the PNAS web site). In Fig. 1*c*, we showed that the CI-M6PR is found in GFP-Ocrl vesicular structures that usually also contain Tf. Whereas only a subset of Tf-positive structures contains GFP-Ocrl, almost all of the CI-M6PR is associated with GFP-Ocrl both at the Golgi and at the endosomes, indicating that Ocrl may be related more to M6PR trafficking than to Tf receptor trafficking. Overall, the microscopy data implicate Ocrl in clathrin-mediated endosomal trafficking. We therefore analyzed the amino acid sequence of Ocrl for conserved binding motifs that are known to mediate interactions to clathrin and clathrin adaptor proteins.

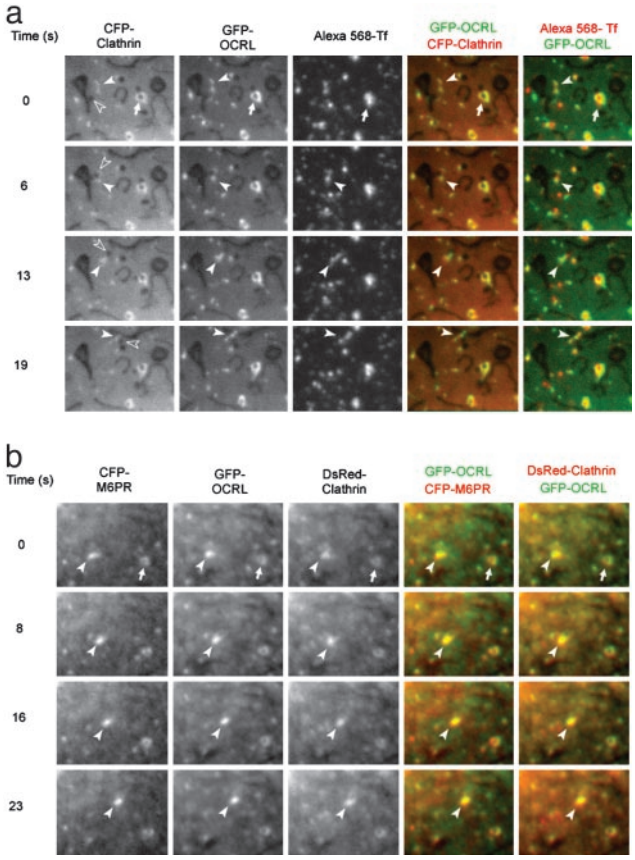

Fig. 3. Proteins associated with Ocrl. (*a*) Live fluorescence microscopy of CFP-clathrin, GFP-Ocrl, and Tf-Alexa 568 after serum stimulation in Cos7 cells. The three proteins colocalize on the large vesicular structure marked by the white arrow. The open arrowhead points at a black vesicular structure that buds off a larger elongated structure. CFP-clathrin, GFP-Ocrl, and Tf-Alexa 568 are found around this budding vesicle (white arrowhead). The three proteins subsequently move with the vesicle toward the top of the picture (see Movie 3). A stationary vesicular structure is marked by an arrow. (*b*) Live fluorescence microscopy of CFP-CD-M6PR, GFP-Ocrl, and DsRed-clathrin after serum stimulation. Two structures that contain all three proteins are pointed out at time 0 s. The structure marked by the arrowhead then moves over the next 23 s; the other vesicular structure remains relatively stationary (see Movie 4).

Ocrl Interacts with the Clathrin Terminal Domain. We found the sequence ^{702}LIDLE, which is an LLDLD-type clathrin box motif, in Ocrl (Fig. 4*a*) (17). Clathrin box motifs can mediate binding to the terminal domain of the clathrin heavy chain. Binding assays with GST-TD show that Ocrl does indeed interact with clathrin (Fig. 4*b*). When we mutated the clathrin box in Ocrl to LIAAA, binding to clathrin was markedly reduced (Fig. 4*b*). The finding that Ocrl interacts with clathrin is consistent with the colocalization of these proteins on endosomes.

Ocrl Binds to the α Appendage Subunit of AP-2 (AP-2α) and Copurifies with Brain CCVs. We next searched for motifs that mediate binding to clathrin adaptor proteins and found that Ocrl contains an FxDxF AP-2 binding motif at residues 151–155 (Fig. 4*a*) but no F/WXXF AP-1 binding motif (18–20). GST binding assays with GST-AP-2α, GST-AP-1γ, and GST-GGA2 (170–613) show that purified Ocrl directly interacts with AP-2α but only slightly with either AP-1γ or GGA2 (Fig. 4*c*). Mutating the ^{151}FEDNF sequence in Ocrl to ^{151}AEANF abolished binding to AP-2α, indicating that the FxDxF motif is required for the interaction between Ocrl and GST-AP-2α (Fig. 4*d*).

Because Ocrl interacts with both clathrin and AP-2, we decided to determine whether Ocrl is a component of CCVs. Synaptosomes were prepared from rat brain homogenate, and CCVs were purified from the synaptosomes. Fractions obtained during purification were analyzed by Western blotting for clathrin, AP-2, hepatocyte growth factor-regulated tyrosine kinase substrate, synaptotagmin, and Ocrl (Fig. 5). The level of Ocrl in different fractions is proportional to that of AP-2 and clathrin. Interestingly, Ocrl is enriched in synaptic CCVs, which are also known to contain the inositol polyphosphate 5-phosphatase synaptojanin-1 (21). To determine whether Ocrl is part of nonneuronal CCVs, we analyzed bovine liver CCVs and found that Ocrl also copurifies with them (data not shown). Because

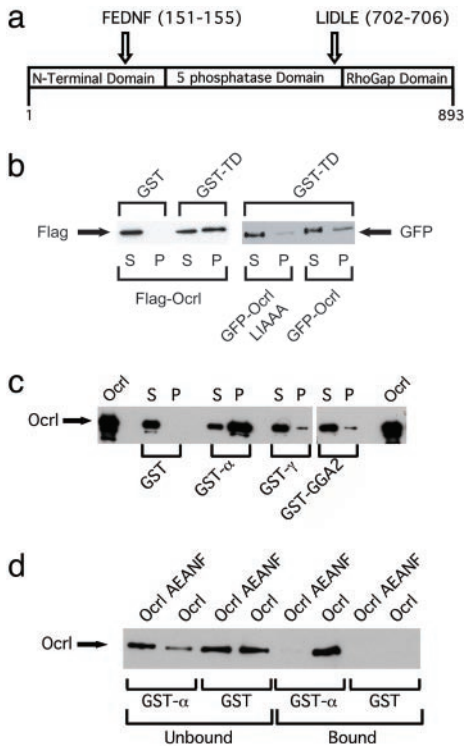

Fig. 4. Ocrl associations. (*a*) Domain structure of Ocrl. Locations of the FEDNF AP-2-binding motif and the clathrin box motif LIDLE are shown. (*b*) Interaction between Ocrl and TD. Flag-Ocrl, GFP-Ocrl, and GFP-Ocrl LIAAA were transiently transfected into HeLa cells. GST or GST-TD beads were incubated with HeLa cell lysates. Sixteen percent of bound (P) and 2% of unbound (S) proteins were analyzed by anti-Flag Western blotting. Fourteen percent of bound (P) and 2% of unbound (S) proteins were analyzed by anti-GFP Western blotting. (*c*) Interaction of purified Ocrl and AP-2α. Ten percent of bound (P) and 1% of unbound (S) fractions of binding assays with GST, GST-α (AP-2α), GST-γ (AP-1γ), and GST-GGA2 (170–613) were analyzed by Ocrl Western blotting. (*d*) Requirement of FxDxF motif in Ocrl for AP-2 binding. Purified Ocrl or Ocrl AEANF mutant protein produced in SF9 cells was incubated with GST or GST-α appendage subunit of AP-2. Ten percent of bound and 1% of unbound fractions were analyzed by Ocrl Western blotting.

Lowe syndrome patients have mental retardation, Ocrl might play an essential role in neuronal trafficking that is different from the function of synaptojanin-1.

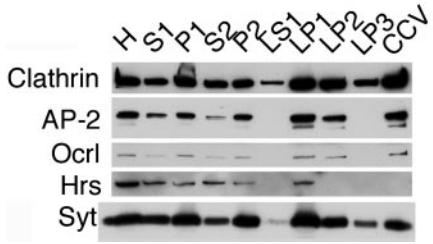

Fig. 5. Ocrl copurifies with CCVs. Fractions were prepared as described by Maycox *et al.* (13). H, homogenate; S1, postnuclear supernatant; P1, nuclei/intact cells/large cell fragments; S2, supernatant minus synaptosomes; P2, crude synaptosomes; LS1, mostly cytosol; LP1, plasma membrane/coated pits/endosomes; LP2, endosomes/synaptic vesicles; LP3, CCV/remaining synaptic vesicles; CCV, highly purified CCV. The amounts of total protein loaded onto gel were as follows: H, 22.5 μg; S1, 8.25 μg; P1, 40.5 μg; S2, 6.4 μg; P2, 9 μg; LS1, 0.75 μg; LP1, 29.25 μg; LP2, 1.95 μg; LP3, 0.75 μg; CCV, 1.8 μg. The blot was probed for clathrin and Ocrl and then stripped and probed for AP-2, the multivesicular endosome marker hepatocyte growth factor-regulated tyrosine kinase substrate (Hrs), and the synaptic vesicle protein synaptotagmin (Syt).

IF studies have shown that AP-2 is found in clathrin-coated pits at the plasma membrane (22), and we do not see colocalization of Ocrl with clathrin-coated pits (data not shown). However, AP-2 has been shown to associate with endosomes in response to epidermal growth factor stimulation in A-431 cells (23). The number of Ocrl-containing endosomes increases after serum stimulation (Fig. 2), and it is possible that Ocrl interacts with AP-2 on endosomal membranes after growth factor stimulation. The function of AP-2 on endosomes remains to be clarified, and future studies are needed to address the significance of the interaction between Ocrl and AP-2.

Discussion

In this paper we present evidence through fixed and live-cell microscopy that Ocrl associates with clathrin-positive endosomes that contain M6PRs and Tf. We also confirm the previously published Golgi localization of Ocrl (14). Ocrl has been localized to lysosomes in kidney epithelial cells (4). This study relied partially on sucrose-treated cells to identify mature lysosomes. Such sucrose-laden structures have subsequently been characterized as lysosome–endosome hybrid structures that contain M6PRs and lamp-2 (24). Because we do not see any overlap between GFP-Ocrl and the lysosomal marker lamp-1, the origin of Ocrl on sucrosomes may have been endosomal rather than lysosomal.

Although GFP-Ocrl is found at the TGN and partially colocalizes with AP-1, we have obtained only weak biochemical evidence for a direct interaction with AP-1 or GGA2 (Fig. 4*c*). Furthermore, the association of Ocrl with Golgi membranes was not affected in AP-1-depleted cells (data not shown). Because AP-1 recruits clathrin to the TGN, it is unlikely that either AP-1 or clathrin recruits Ocrl to Golgi membranes (25). It will be important to determine whether Ocrl is on TGN-derived CCVs, an issue best approached with immunogold electron microscopy. It was recently shown that phosphatidylinositol-4-phosphate is important for the recruitment of the AP-1 complex to Golgi membranes (8). Previous data have implicated a role for PtdIns-4,5-P_2 in the formation of CCVs at the TGN (7, 9). It is possible that Ocrl is converting pools of PtdIns-4,5-P_2 to phosphatidylinositol-4-phosphate to regulate the formation of M6PR-containing CCVs.

Data presented in this paper raise the possibility that Ocrl functions on clathrin-, Tf-, and M6PR-positive endosomes. The number of CFP-clathrin-positive and GFP-Ocrl-positive endosomes in the cytoplasm was increased upon serum stimulation. This finding is consistent with data showing that epidermal growth factor stimulation can lead to increased association of clathrin, AP-1, and AP-2 with endosomes (23). After serum stimulation, the cells rapidly internalize ligand-activated receptors by receptor-mediated endocytosis (26). The accumulation of membranes inside the cell might lead to an increase in number and size of endosomal compartments. Furthermore, the large number of receptors that are being internalized will require a high level of sorting, in which Ocrl, clathrin, and clathrin adaptors might be participating. We therefore routinely starve and subsequently serum-stimulate cells for imaging to increase the number of GFP-Ocrl-positive endosomal structures per cell. The clathrin on the endosomes appears to be relatively stable over time, although it does move around the endosomal membrane. An important issue to be addressed is whether we are imaging clathrin-coated buds or the bilayered clathrin that has been implicated in the sorting of receptors into multivesicular bodies (27–29). We also plan to test whether Ocrl and AP-2 colocalize on endosomal membranes in response to serum stimulation.

How Ocrl might affect endosomal trafficking and the trafficking of which cargo molecules is regulated by Ocrl remains to be clarified. We show that Ocrl binds to clathrin and AP-2, and

it is possible that Ocrl regulates the association of those proteins with endosomes. To determine whether Ocrl may be involved in the recycling of plasma membrane receptors at the endosome, we measured the recycling of ^{125}I-Tf in cells that were either transfected with Ocrl small interfering RNA or GFP-Ocrl. Neither transfection affected the recycling of Tf (data not shown). This finding is consistent with the microscopic data, which show that whereas GFP-Ocrl-positive endosomes usually contain Tf, only a small proportion of Tf-positive structures contain GFP-Ocrl (Fig. 1*b*). In contrast, GFP-Ocrl is found on nearly all M6PR-containing endosomes (Fib. 1*c*), suggesting that Ocrl functions together with clathrin in the sorting of the M6PRs rather than in the recycling of the Tf receptors. Thus, the redistribution of AP-1 and M6PRs in cells overexpressing Ocrl may be due to defective transport from endosomes back to the TGN rather than a direct effect at the Golgi (Fig. 6). Lowe-syndrome patients have twice the activity of lysosomal enzymes in plasma as do controls (6), and abnormal trafficking of lysosomal enzymes may contribute to the phenotype of Lowe syndrome. However, it is likely that other intracellular trafficking pathways are affected as well. Interestingly, the major substrate of Ocrl, PtdIns-4,5-P_2, is known to regulate the actin cytoskeleton, which is essential for lysosomal enzyme trafficking (30). A cytoskeletal defect in Lowe-syndrome-patient fibroblasts has been described and may contribute to abnormal vesicular transport in patients (31).

In summary, our results support a role for Ocrl in endosomal trafficking. Future studies on the exact role of Ocrl in vesicular transport may lead to a better understanding of the complex pathophysiology of Lowe syndrome.

We thank Cecil Buchanan, Beate Grossmann, and Huberta Ungewickell for excellent technical assistance; Monita Wilson, Shao-Chung Chang, John Verbsky, Chris Hugge, Balraj Doray, George Broze III, and Marina Kisseleva for helpful discussions; and our colleagues Frances Brodsky, Lois Greene, Jim Keen, Stuart Kornfeld, and Suzanne Pfeffer for supplying reagents. This work was supported by American Heart Association Grant 0415283Z (to A.U.), Deutsche Forschungsgemeinschaft Grant UN 43/5-1 (to E.U.), and National Institutes of Health Grants HL 55272, HL 16634, and H107088 (to P.W.M.).

1. Attree, O., Olivos, I. M., Okabe, I., Bailey, L. C., Nelson, D. L., Lewis, R. A., McInnes, R. R. & Nussbaum, R. L. (1992) *Nature* **358,** 239–242.
2. Nussbaum, R. (2000) in *The Metabolic and Molecular Bases of Inherited Disease*, eds. Scriver, C. R., Sly, W.S., Childs, B., Beaudet, A. L., Valle, D., Kinzler, K. W. & Vogelstein, B. (McGraw–Hill, New York), 8th Ed., pp. 6257–6266.
3. Majerus, P. W., Kisseleva, M. V. & Norris, F. A. (1999) *J. Biol. Chem.* **274,** 10669–10672.
4. Zhang, X., Hartz, P. A., Philip, E., Racusen, L. C. & Majerus, P. W. (1998) *J. Biol. Chem.* **273,** 1574–1582.
5. Suchy, S. F., Olivos-Glander, I. M. & Nussbaum, R. L. (1995) *Hum. Mol. Genet.* **4,** 2245–2250.
6. Ungewickell, A. J. & Majerus, P. W. (1999) *Proc. Natl. Acad. Sci. USA* **96,** 13342–13344.
7. De Matteis, M., Godi, A. & Corda, D. (2002) *Curr. Opin. Cell Biol.* **14,** 434–447.
8. Wang, Y. J., Wang, J., Sun, H. Q., Martinez, M., Sun, Y. X., Macia, E., Kirchhausen, T., Albanesi, J. P., Roth, M. G. & Yin, H. L. (2003) *Cell* **114,** 299–310.
9. Crottet, P., Meyer, D. M., Rohrer, J. & Spiess, M. (2002) *Mol. Biol. Cell* **13,** 3672–3682.
10. Ghosh, P., Dahms, N. M. & Kornfeld, S. (2003) *Nat. Rev. Mol. Cell Biol.* **4,** 202–212.
11. Dressman, M. A., Olivos-Glander, I. M., Nussbaum, R. L. & Suchy, S. F. (2000) *J. Histochem. Cytochem.* **48,** 179–190.
12. Huttner, W. B., Schiebler, W., Greengard, P. & De Camilli, P. (1983) *J. Cell Biol.* **96,** 1374–1388.
13. Maycox, P. R., Link, E., Reetz, A., Morris, S. A. & Jahn, R. (1992) *J. Cell Biol.* **118,** 1379–1388.
14. Olivos-Glander, I. M., Janne, P. A. & Nussbaum, R. L. (1995) *Am. J. Hum. Genet.* **57,** 817–823.
15. Jefferson, A. B. & Majerus, P. W. (1996) *Biochemistry* **35,** 7890–7894.
16. Keyel, P. A., Watkins, S. C. & Traub, L. M. (2004) *J. Biol. Chem.* **279,** 13190–13204.
17. Kirchhausen, T. (2000) *Annu. Rev. Biochem.* **69,** 699–727.
18. Bai, H., Doray, B. & Kornfeld, S. (2004) *J. Biol. Chem.* **279,** 17411–17417.
19. Brett, T. J., Traub, L. M. & Fremont, D. H. (2002) *Structure (London)* **10,** 797–809.
20. Mattera, R., Ritter, B., Sidhu, S. S., McPherson, P. S. & Bonifacino, J. S. (2004) *J. Biol. Chem.* **279,** 8018–8028.
21. Cremona, O., Di Paolo, G., Wenk, M. R., Luthi, A., Kim, W. T., Takei, K., Daniell, L., Nemoto, Y., Shears, S. B., Flavell, R. A., *et al.* (1999) *Cell* **99,** 179–188.
22. Ahle, S., Mann, A., Eichelsbacher, U. & Ungewickell, E. (1988) *EMBO J.* **7,** 919–929.
23. Sorkina, T., Bild, A., Tebar, F. & Sorkin, A. (1999) *J. Cell Sci.* **112,** 317–327.
24. Bright, N. A., Reaves, B. J., Mullock, B. M. & Luzio, J. P. (1997) *J. Cell Sci.* **110,** 2027–2040.
25. Meyer, C., Zizioli, D., Lausmann, S., Eskelinen, E. L., Hamann, J., Saftig, P., von Figura, K. & Schu, P. (2000) *EMBO J.* **19,** 2193–2203.
26. Marmor, M. D. & Yarden, Y. (2004) *Oncogene* **23,** 2057–2070.
27. Raiborg, C., Bache, K. G., Gillooly, D. J., Madshus, I. H., Stang, E. & Stenmark, H. (2002) *Nat. Cell Biol.* **4,** 394–398.
28. Raiborg, C., Bache, K. G., Mehlum, A., Stang, E. & Stenmark, H. (2001) *EMBO J.* **20,** 5008–5021.
29. Sachse, M., Urbe, S., Oorschot, V., Strous, G. J. & Klumperman, J. (2002) *Mol. Biol. Cell* **13,** 1313–1328.
30. Carreno, S., Engqvist-Goldstein, A. E., Zhang, C. X., McDonald, K. L. & Drubin, D. G. (2004) *J. Cell Biol.* **165,** 781–788.
31. Suchy, S. F. & Nussbaum, R. L. (2002) *Am. J. Hum. Genet.* **71,** 1420–1427.